IEEE Access
Multidisciplinary | Rapid Review | Open Access Journal

Received 14 November 2022, accepted 7 December 2022, date of publication 21 December 2022,
date of current version 29 December 2022.

Digital Object Identifier 10.1109/ACCESS.2022.3231457

RESEARCH ARTICLE

Monolithically Fabricated Waveguide for Efficient Guiding and Emission of Visible Light for IoT Applications

HYUN JIN JUNG[1], UI SEOK JUNG[1,2], BYUNG CHUL LEE[3,4,5], (Member, IEEE), AND SOO JIN KIM[1]

[1]School of Electrical Engineering, Korea University, Seoul 02841, Republic of Korea
[2]NAND Process Integration, SK Hynix, Icheon-si 17336, Republic of Korea
[3]Bionics Research Center, Korea Institute of Science and Technology (KIST), Seoul 02792, Republic of Korea
[4]Division of Bio-Medical Science and Technology, KIST School, University of Science and Technology (UST), Seoul 02792, Republic of Korea
[5]KHU-KIST Department of Converging Science and Technology, Kyung Hee University, Seoul 02447, Republic of Korea

Corresponding author: Soo Jin Kim (kimsjku@korea.ac.kr)

This work was supported in part by the National Research Foundation of Korea (NRF) Grant Funded by the [Ministry of Science and ICT of Korea Government (MSIT)] under Grant NRF-2022R1A2C4001246 and Grant NRF-2022R1A4A1034315 and in part by Korea University Grant.

ABSTRACT We present monolithically integrated waveguide with thin isolated layers of dielectric material, which ensure efficient emission of guided light in multiple optical windows. The proposed waveguide is fabricated by using silicon oxynitride (SiON) which functions as the core guiding layer, and silicon nitride (SiN) which facilitates effective vertical emission of guided light via optical windows. The theoretical operating principle is analyzed by Finite-Difference-Time-Domain (FDTD) simulation, and the experimentally fabricated device is demonstrated to find the expected operational trend by measuring vertical emission of light through the optical windows. We further find that the physical origin of such efficient emission stems from the Fabry-Perot resonance induced laterally at the interface between the optical windows and cladding layers, which leads to the strong emission of light at the edge of optical windows. The output efficiencies of light emission from SiN optical windows, which are fabricated in cascaded fashion on top of the SiON waveguide, are 30, 45 and 55 percent at the wavelength of 457, 532, and 637 nm, respectively. The proposed design concept can be applied to various potential applications including optical integrated circuits with vertical interconnection, optical emission in wearable devices for virtual and augmented reality, and other emerging optical sensors.

INDEX TERMS Optical window, vertical emission, optical integrated circuit, wearable devices.

I. INTRODUCTION

For the past decades, photonic devices have been considered and utilized as essential building blocks for optical on-chip technology by transmitting and modulating optical signals [1], [2], [3], [4], [5], [6]. More recently, the application of photonic elements, including waveguides, has expanded in more diverse fields such as communications [7], [8], biosensing [9], photodetectors [10], [11], and modulators [12]. In particular, emerging fields of the internet of things (IoT) applications which include augmented and virtual reality (AR and VR), on-chip biosensor and next-generation optical circuits, need a new concept of optical elements which are different from the conventional ones in terms of operating principle, wavelengths, and designed structure. For instance, there is growing interest in the design of a conceptually new waveguide which is capable of emitting guided light into free space in the lateral and vertical direction for a designer application, and this requires the entirely different concept of waveguide design from the conventional one that uses diffraction gratings for free space coupling [13], [14], [15], [16], [17]. Unlike the conventional silicon waveguide, various IoT devices or emerging optical circuits integrate waveguide to precisely locate the emission of light while simultaneously

The associate editor coordinating the review of this manuscript and approving it for publication was Leo Spiekman.

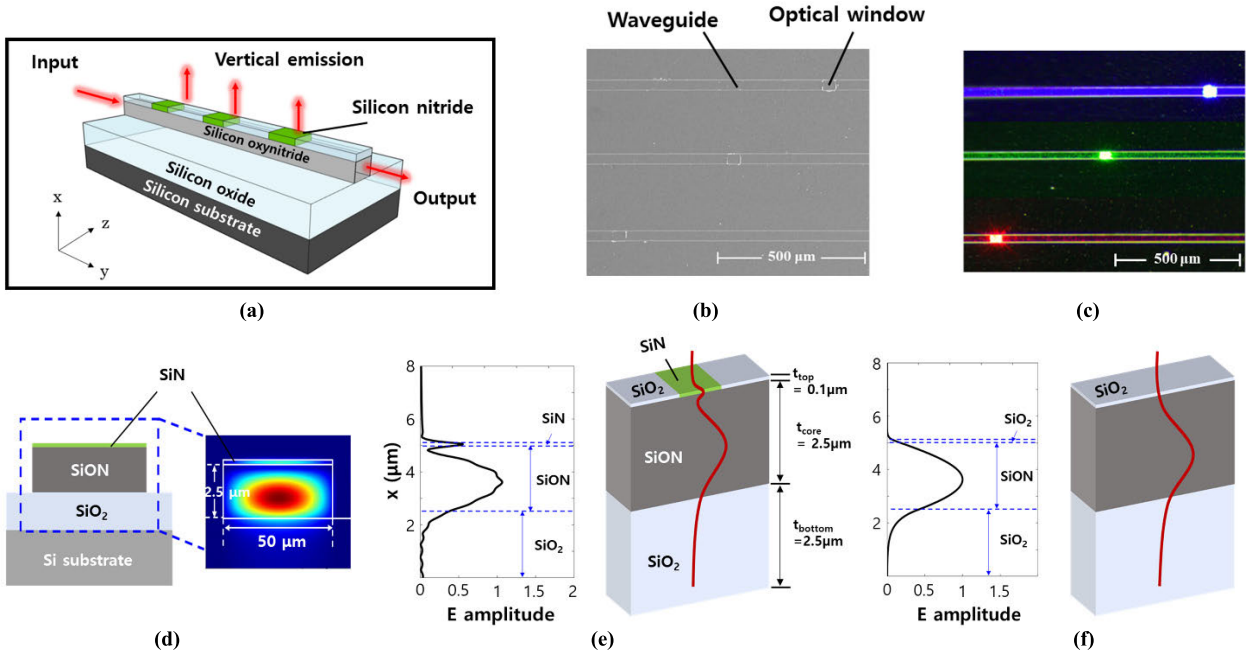

FIGURE 1. Silicon oxynitride (SiON) based waveguide for lossless control of visible light and vertical, free space emission for mutli-channel applications (a) The schematic diagram of the SiON waveguide with multiple emission via silicon nitride (SiN) based optical windows. (b) SEM image of fabricated, three representative SiON waveguides (tilted view). (c) Optical image of the waveguides and vertical emission via SiN windows at the operating wavelengths of 457 nm, 532 nm and 637 nm. (d) Spatial distribution of resonant modes along the waveguide direction for fundamental TM mode, (e-f) Amplitudes of electric fields in SiON waveguide with/without SiN windows.

guiding the partial energy of light in the waveguide for multiple point displaying or sensing functions. To achieve such functionality, considerable research has been conducted to realize the new concept of waveguide by patterning the surface of the emitter or extraordinarily fabricating the device. Examples of these include the design of metasurfaces by patterning the structures in subwavelength size [18], [19], [20], [21], [22], [23] or fabricating the waveguide itself as a three-dimensional cantilever shape [24], [25], [26], [27], which effectively controls the light emission, however, with the limited applications due to the complexity of fabrication and efficiency.

Meanwhile, as an additional requirement to the waveguide for the applications to the various sensing and internet of things (IoT) systems, the waveguide needs to be effectively operated at the designer spectral signal including visible and near-infrared bands. For instance, in a wearable display application, waveguide requires guiding visible light without inducing any intrinsic absorption loss in constituent materials [28], [29]. Unlike the silicon-based one, the guiding material needs to be lossless with high bandgap energy to satisfy such condition.

Thus, there are needs to realize a new waveguiding system capable of emitting light at the designer locations of multiple channels vertically or laterally with simultaneous guiding of light. Also, the designed waveguide should be loss-free at the operating spectral range, including visible light for on-demand applications. In this work, we present a new type of waveguide fabricated using silion oxynitride (SiON) for the lossless control of visible light. Such device is monolithically integrated with silicon nitride (SiN) optical windows for effective vertical emission of light at the designer location in the waveguide.

II. DESIGN AND SIMULATED ANALYSIS

The proposed device is schematically illustrated in Fig. 1(a). The designed optical waveguide consists of a core guiding layer and multiple optical windows monolithically fabricated on top of the guiding layer. The pad-shaped optical windows afford effective vertical light emission while simultaneously guiding light for multiple emissions in various designer positions. The core guiding layer and the cladding layer surrounding the core layer are SiON and SiO_2 with the refractive index of 1.48 (n=1.48) and 1.45 (n=1.45), respectively. We designed the waveguide using SiON which has the advantage of the lossless nature of guiding in visible wavelength and tunable refractive index by changing the rate of oxygen and nitrogen [30]. Based on the fabrication optimization of our previous works [31], we realize the SiON waveguide which is capable of vertically emitting light in multiple waveguide windows, as described in Fig. 1(a). To effectively realize this and monolithically fabricate the device in a micro-scale, we designed the pad-shaped optical windows for the light emission using SiN with the refractive index of 2. The optical field is effectively confined at the SiON waveguide and split into the isolated SiN optical windows with the higher refractive index than SiON. Fig. 1(b) shows the scanning electron microscopy (SEM) image of the

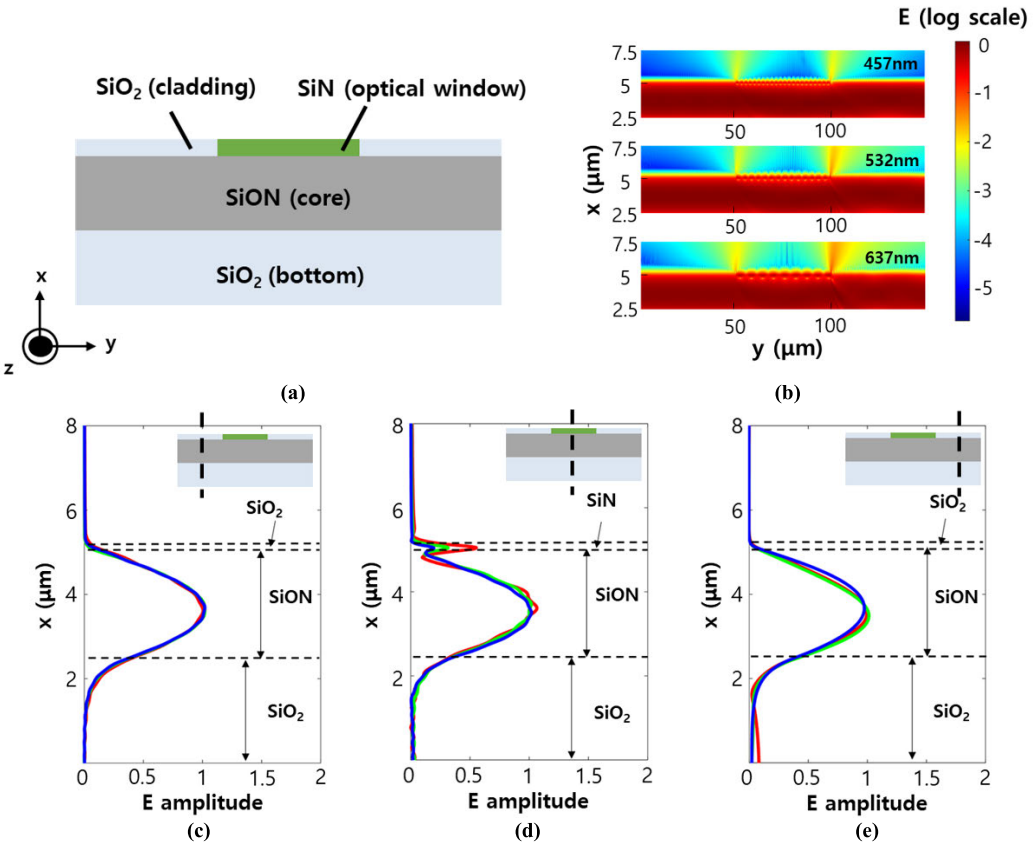

FIGURE 2. Simulated analysis of SiON waveguide and physical origin of light emission in the SiN windows (a) The cross sectional diagram of an waveguide with optical window. Simulation is conducted at the wavelengths of 457, 532 and 637 nm. (b) Profile of electric field diplaying vertical emission at the edge region of isolated optical window. (c-e) Electric field amplitude along the vertical direction at three representative locations indicated at the inset images of waveguide.

fabricated waveguides integrated with the optical window layer. This figure is viewed from the top of the waveguide chip, and the isolated SiN layer is fabricated with the size of 50 by 50 μm. Fig. 1(c) shows the optical images of fabricated samples coupled with the light source at the wavelengths of 457, 532 and 637 nm, respectively. It is clearly observed from the images that the guided light is effectively coupled to the isolated SiN layers and emitted vertically into free space.

To theoretically analyze the designed waveguide, we performed full field simulation using the Finite Difference Time Domain (FDTD) method. Figure 1(d) shows the waveguide's cross-section and the electric field distribution at the wavelength of 632nm. The guided electric field with the fundamental transverse magnetic (TM) mode is effectively confined in the core guiding layer of SiON with the partial energy coupled and concentrated at the thin layer of the SiN optical window. Fig 1(e) depicts the amplitudes of the normalized electric field along the vertical direction from the SiN layer to the bottom SiO_2 cladding layer. The thickness of the bottom cladding layer (t_{bottom}), the core guiding layer, and the optical window (t_{top}) are 2.5μm, 2.5 μm, and 100 nm, respectively. Compared to the example without the SiN layer (Fig. 1(f)), the designed waveguide shows the pronounced electric field enhancement at the very thin layer of SiN at the top, which affords the change of the momentum of the guided light and enables the efficient vertical emission. From the analysis, it is clear that the presence of the SiN layer with the higher refractive index could facilitate the efficient vertical emission of light.

As the next stage, we study the detailed operating principle of vertical emission by investigating the field pattern at the SiN windows. Fig. 2(a) shows the schematics of the waveguide along the guiding direction, and Fig. 2(b) shows the electric field profiles of waveguides viewed from the schematic perspective. The designed parameters of the structure, including thickness, width, and materials, are the same as in Fig. 2(a), and wavelengths of the guided light are 457, 532, and 637nm. From the analysis, it is clearly observed that the electric field is maximally and effectively emitted from the edge of the SiN layers, which indicates that the large portion of the emission occurred near the boundary than the central window region. In addition, a standing wave pattern is observed in the thin SiN layer illustrating the combination of the nodes and anti-nodes of the electric field. The excitation of Fabry-Perot resonance causes this in the lateral direction along the SiN layer. From the analysis, it is

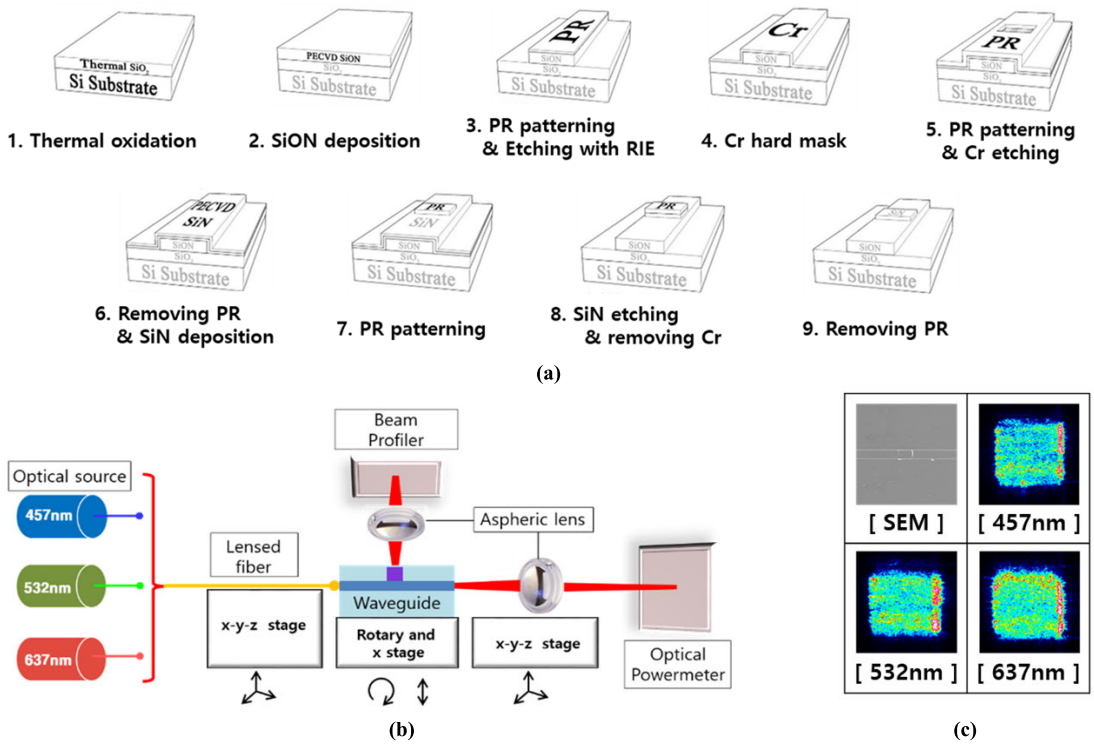

FIGURE 3. Microfabrication procedures of the SiON waveguide with SiN windows and measurement setup for the optical analysis. (a) CMOS micro fabrication process of the waveguide. (b) A schematic diagram of the optical measurement system. (c) SEM image and the images of optical beam distributions at the SiN optical window by using beam profiler.

concluded that the guided light is effectively coupled to the isolated SiN layer which excites the lateral Fabry-Perot resonance and enables the effective vertical emission as the light is scattered at the interfaces near the edge of the optical windows. The results of the calculated electric fields at each wavelength are shown in Fig. 2(c), (d), and (e). The electric fields of input waves are confined as a sinusoidal shape at the core region initially before the light encounter the SiN optical window. As the wave propagates to the SiN layer, the electric field is pronouncedly enhanced in the thin window layers at each launched three wavelengths. Additional analysis of higher order guided mode is evaluated in supplementary materials.

III. EXPERIMENTAL DEMONSTRATIONS

To experimentally demonstrate the vertical emission and aforementioned analysis of the edge effect, we fabricated the waveguide and measured the power and optical images of emission profiles. We start by fabricating the SiON waveguide with a thin SiN pad using the micro-fabrication techniques. A detailed fabrication process for the device is shown in Fig. 3(a). The bottom cladding layer is formed with the thermal oxidation of a silicon wafer to produce a SiO_2 with a refractive index of 1.458 and a thickness of 2.5 μm. The core guiding layer of SiON is fabricated by PECVD processes with the given gas flow ratios of 50 sccm N_2O and 150 sccm SiH_4 [31]. A core layer of SiON with a refractive index of 1.475 is then deposited at a thickness of 2.5 μm by using the PECVD process. The photolithography is performed after the spin-coat of AZ 4620 photoresist (PR) and the core layer is etched using reactive ion etching (RIE) with a mixture of CF_4 and O_2 gas for forming the fine core of waveguide. To make the optical window patterns while preventing damage of the core layer in the waveguide, a 2500-Å thick chromium (Cr) layer is used, which is deposited by using an e-beam evaporator. AZ 4620 PR is used as a photolithographic mask, and the Cr hard mask is patterned by wet chemical etching with a CR-7 solution (Cyantek Co., Fermont, Calif.). After removing the PR, a SiN layer is deposited at a thickness of 100 nm by using PECVD. To make the optical window of SiN, the square shapes are patterned by photolithography after the PR deposition. The optical window is etched using RIE with a mixture of CF_4 and O_2 gas. The PR is removed, and the waveguide is cleaned by 1:1 (H_2SO_4: H_2O_2) solution for 10 minutes. Finally, the 2.5 μm thick-SiON waveguide core (refractive index of 1.461) is realized, which is surrounded by SiO_2 as the cladding layers and SiN as the optical window layers. The optical characteristics of the waveguides were measured by an optical measurement system, as shown in Fig. 3(b). The lasers (diode-pumped solid-state and laser diode), which respectively have 457 nm (457 LB series, LaserLab Co.), 532 nm (532 LB series, LaserLab Co.) and 637 nm (LP635-SF8, Thorlabs Co.)

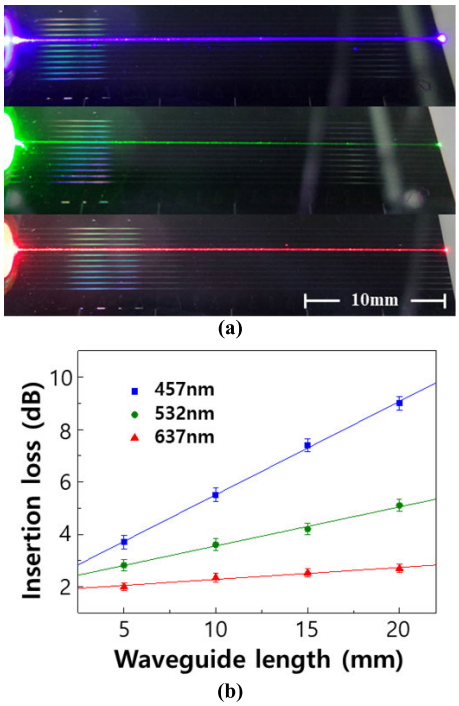

FIGURE 4. Optical characteristics of SiON waveguides at 457nm, 532nm, 637nm wavelengths. (a) Optical images of light propagation in the fabricated waveguides. (b) Insertion loss in the SiON waveguide for various lengths of waveguides.

wavelengths, were utilized as light source. The light was aligned with a piezoelectric translational stage (MAX312D, Thorlabs Co.) to the waveguide and coupled in the waveguide with a lensed fiber. The coupled light propagates through the path of the waveguide and is emitted from the end facet of the waveguide device. Transmitted light passed through the aspheric lens (C392TME-A, Thorlabs Co.) and arrived at an optical power meter. To confirm the vertical emission in optical windows, the qualitative analysis was carried out by taking the image with a CCD (charge-coupled device) camera, which is visualized in Fig. 3(c). In Fig. 3(c), we visualize the optical images of vertical emission at the three representative wavelengths at a specific optical window indicated in the SEM image. From the measurements, it is verified that there are effective vertical emissions in the SiN windows with the enhanced efficiency near the edge region, which matches well with the trend of the simulated analysis.

Next, we experimentally evaluate the waveguiding performance and emission in the optical windows by measuring the transmitted power from the fabricated waveguides. First, the insertion loss of the SiON waveguide is measured by using the cutback method. For the measurement, the waveguide without the vertically opened optical window is utilized. And the waveguides are prepared with the length of 20 mm. The results of propagated lights at the wavelength of 457, 532, and 637 nm and the insertion loss measurements are shown in Fig. 4. As shown in Fig. 4(a) which shows the representative optical images, the guided light is properly propagated at the

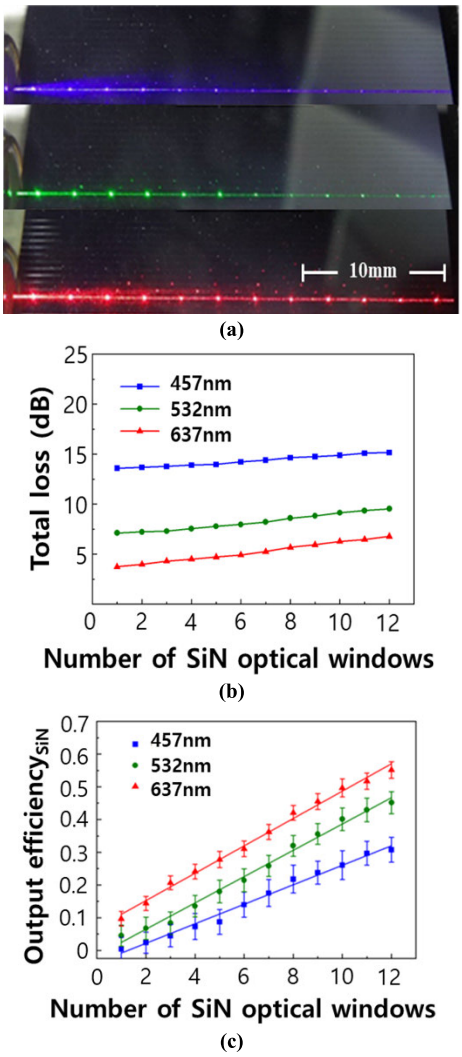

FIGURE 5. Optical characteristics of SiN/SiON waveguide at 457nm, 532nm, 637nm wavelengths. (a) Optical image of the three representative waveguides with the SiN optical windows. The length of waveguide is 30 cm. (b) Measured total loss in the waveguides with multiple number of SiN optical windows. (c) Output efficiency of SiN optical window emission.

waveguide and emitted at the opposite end of waveguide. The measured coupling losses are 1.95, 2.07, and 1.83 dB at the wavelength of 457, 532, and 637 nm, respectively. The slight difference in the coupling loss is mainly caused by the imperfect formation of the focal beam shapes. The measured propagation losses are 3.56, 1.49, and 0.46 dB/cm at each wavelength, as shown in Fig. 4(b). The propagation loss can be explained mainly by the effect of the rough surfaces of fabricated waveguide [32]. As a result, the loss is monotonically increased as the wavelength of the inserted light decreases.

Finally, the efficiency of the optical emission in the SiN windows is measured and evaluated, as shown in Fig. 5. Fig. 5(a) shows the optical images of the waveguide with twelve SiN optical windows which enable the effective light emission into free space. The optical power from the optical

window is measured using the optical systems directly. Fig. 5(b) shows the total loss measured from the fabricated waveguide systems based on the values of the insertion and radiation loss. Specifically, the total loss is expressed as follows,

$$\begin{aligned}\text{Total loss (dB)} = &\ [\text{radiation loss (via windows (watt))} \\ &+ \text{insertion loss} \\ &(\text{w/o windows (watt))}\ ]\ (\text{dB}) \end{aligned} \quad (1)$$

where the radiation loss is measured directly above the SiN windows using the optical power meter and the insertion loss is estimated from the bare waveguide using the cutback method based measurements. It is observed from Fig 5(b) that a substantial portion of loss stems from the insertion loss due to the imperfect and non-ideal fabrication of the waveguides, and the additional increment of loss originates from the vertical emission of light in the SiN windows. To essentially evaluate the effectiveness of the vertical emission, the optical power emitted from the optical windows are directly measured and estimated as exhibited in Fig 5(c). Note that the output efficiency of the optical window (output efficiency $_{\text{SiN}}$) is defined as the ratio of the optical power emitted from the SiN windows (output $_{\text{SiN}}$) to the reference power transmitted to the end at the waveguide without the optical windows (output $_{\text{SiON}}$).

$$\text{Output efficiency}_{\text{SiN}} = \frac{\text{output}_{\text{SiN}}(\text{watt})}{\text{output}_{\text{SiON}}(\text{watt})} \quad (2)$$

It is observed from the figure that the output efficiency is gradually increased as the emitted power is monotonically weighted by the addition of optical windows. In addition, such a gradual increase implies that light is partially emitted at each SiN window and partially propagated in the waveguide to the end. Although the emission power from the first SiN window is slightly higher than the consequent cascaded windows, the overall emission of power at each SiN window is not significantly changed and follows the approximated straight guideline depicted in Fig 5(c), which indicates that the uniform emission of light from 12 isolated window regions. The net output efficiencies of 12 SiN windows are 30, 45, and 55 % at the wavelength of 457, 532, and 637 nm, respectively.

IV. CONCLUSION

We present the optical waveguide integrated with SiN-based isolated optical windows, which ensure efficient and near uniform multiple emission of light. To understand the operating principle and optimal design, we perform an in-depth analysis of the phenomena of the vertical emission in the SiN windows to find the pronounced effect near the edge of the designed pad, which is caused by the lateral directional resonances occurring in a very thin SiN layer. We verify the underlying physics and performance by measuring the optical power from the SiN-integrated waveguide samples which are successfully fabricated using micro-CMOS fabrication methods. The proposed and fabricated design concept can be applied in diverse applications including wearable optical sensors, displays, and potential optical on-chip integration.

REFERENCES

[1] H. Mekawey, M. Elsayed, Y. Ismail, and M. A. Swillam, "Optical interconnects finally seeing the light in silicon photonics: Past the hype," *Nanomaterials*, vol. 12, no. 3, p. 485, Jan. 2022.
[2] A. E. Willner, S. Khaleghi, M. R. Chitgarha, and O. F. Yilmaz, "All-optical signal processing," *J. Lightw. Technol.*, vol. 32, no. 4, pp. 660–680, Feb. 15, 2014.
[3] L. Chen, C. Doerr, R. Aroca, J. Heanue, T. Nielsen, S. Azemati, G. Ali, L. Chen, B. Guan, and H. Zhang, "Silicon photonics in optical coherent systems," in *Proc. 23rd Opto-Electron. Commun. Conf. (OECC)*, Jul. 2018, pp. 2291–2301.
[4] J. Guo and D. Dai, "Silicon nanophotonics for on-chip light manipulation," *Chin. Phys. B*, vol. 27, no. 10, Oct. 2018, Art. no. 104208.
[5] S. Kaushal, R. Cheng, M. Ma, A. Mistry, M. Burla, L. Chrostowski, and J. Azaña, "Optical signal processing based on silicon photonics waveguide Bragg gratings: Review," *Frontiers Optoelectron.*, vol. 11, no. 2, pp. 163–188, Jun. 2018.
[6] Y. Meng, Y. Chen, L. Lu, Y. Ding, A. Cusano, J. A. Fan, Q. Hu, K. Wang, Z. Xie, Z. Liu, Y. Yang, Q. Liu, M. Gong, Q. Xiao, S. Sun, M. Zhang, X. Yuan, and X. Ni, "Optical meta-waveguides for integrated photonics and beyond," *Light, Sci. Appl.*, vol. 10, no. 1, pp. 1–44, 2021.
[7] C. Xiong, W. H. P. Pernice, and H. X. Tang, "Low-loss, silicon integrated, aluminum nitride photonic circuits and their use for electro-optic signal processing," *Nano Lett.*, vol. 12, no. 7, pp. 3562–3568, Jul. 2012.
[8] U. Jeong, D. H. Lee, K. Lee, and J. H. Park, "Monolithic 1 × 8 DWDM silicon optical transmitter using an arrayed-waveguide grating and electro-absorption modulators for switch fabrics in intra-data-center interconnects," *Micromachines*, vol. 11, no. 11, p. 991, Nov. 2020.
[9] S. Sahu, J. Ali, P. P. Yupapin, and G. Singh, "Optical biosensor based on a cladding modulated grating waveguide," *Optik*, vol. 166, pp. 103–109, Aug. 2018.
[10] A. Chatterjee, S. Yadav, S. K. Sikdar, and S. K. Selvaraja, "High-speed cavity enhanced silicon photodetector on SiN-SOI platform for short reach optical datacom," in *Proc. Workshop Recent Adv. Photon. (WRAP)*, Dec. 2019, pp. 1682–1685.
[11] K. Ohira, K. Kobayashi, N. Iizuka, H. Yoshida, M. Ezaki, H. Uemura, A. Kojima, K. Nakamura, H. Furuyama, and H. Shibata, "On-chip optical interconnection by using integrated III–V laser diode and photodetector with silicon waveguide," *Opt. Exp.*, vol. 18, no. 15, pp. 15440–15447, Jul. 2010.
[12] H. Xu, X. Li, X. Xiao, P. Zhou, Z. Li, J. Yu, and Y. Yu, "High-speed silicon modulator with band equalization," *Opt. Lett.*, vol. 39, no. 16, pp. 4839–4842, 2014.
[13] X. Chen, C. Li, C. K. Y. Fung, S. M. G. Lo, and H. K. Tsang, "Apodized waveguide grating couplers for efficient coupling to optical fibers," *IEEE Photon. Technol. Lett.*, vol. 22, no. 15, pp. 1156–1158, Aug. 1, 2010.
[14] J. Jian, P. Xu, H. Chen, M. He, Z. Wu, L. Zhou, L. Liu, C. Yang, and S. Yu, "High-efficiency hybrid amorphous silicon grating couplers for sub-micron-sized lithium niobate waveguides," *Opt. Exp.*, vol. 26, no. 23, pp. 29651–29658, Nov. 2018.
[15] Y. Ding, H. Ou, and C. Peucheret, "Ultrahigh-efficiency apodized grating coupler using fully etched photonic crystals," *Opt. Lett.*, vol. 38, no. 15, pp. 2732–2734, 2013.
[16] Z. Zhao and S. Fan, "Design principles of apodized grating couplers," *J. Lightw. Technol.*, vol. 38, no. 16, pp. 4435–4446, Aug. 15, 2020.
[17] C.-S. Im, B. Bhandari, K.-P. Lee, S.-M. Kim, M.-C. Oh, and S.-S. Lee, "Silicon nitride optical phased array based on a grating antenna enabling wavelength-tuned beam steering," *Opt. Exp.*, vol. 28, no. 3, pp. 3270–3279, Feb. 2020.
[18] A. Yaacobi, E. Timurdogan, and M. R. Watts, "Vertical emitting aperture nanoantennas," *Opt. Lett.*, vol. 37, no. 9, pp. 1454–1456, May 2012.
[19] Y. S. Zeng, S. W. Qu, C. Wang, B. J. Chen, and C. Chan, "Efficient unidirectional and broadband vertical-emitting optical coupler assisted by aperture-coupled nanopatch antenna array," *Opt. Exp.*, vol. 27, no. 7, pp. 9941–9954. 2019.
[20] Y. Zeng, S. Qu, and J. Wu, "Polarization-division and spatial-division shared-aperture nanopatch antenna arrays for wide-angle optical beam scanning," *Opt. Exp.*, vol. 28, no. 9, pp. 12805–12826, 2020.

[21] J. Park, S. J. Kim, V. J. Sorger, and S. J. Kim, "Electrically tunable metasurface by using InAs in a metal–insulator–metal configuration," *Nanophotonics*, vol. 11, p. 1117, Feb. 2022.
[22] H. Kim, "Numerical studies on antiresonant waveguide assisted metasurface and its application," *IEEE Access*, vol. 10, pp. 75949–75955, 2022.
[23] J. Park, "All-solid-state spatial light modulator with independent phase and amplitude control for three-dimensional LiDAR applications," *Nature Nanotechnol.*, vol. 16, no. 1, pp. 69–75, 2021.
[24] Y. Jing, G. Fan, R. Wang, Z. Zhang, X. Cai, J. Wei, X. Chen, H. Li, and Y. Li, "Improved optical waveguide microcantilever for integrated nanomechanical sensor," *Sensors*, vol. 19, no. 19, p. 4346, Oct. 2019.
[25] A. Z. Subramanian, "Low-loss singlemode PECVD silicon nitride photonic wire waveguides for 532–900 nm wavelength window fabricated within a CMOS pilot line," *IEEE Photon. J.*, vol. 5, no. 6, Dec. 2013, Art. no. 2202809.
[26] K. Zinoviev, C. Dominguez, J. A. Plaza, and L. M. Lechuga, "Optical waveguide cantilever actuated by light," *Appl. Phys. Lett.*, vol. 92, no. 1, pp. 011908-1–011908-3, Jan. 2008.
[27] Y. Jing, G. Fan, R. Wang, Z. Zhang, M. Wang, X. Cai, J. Wei, X. Chen, H. Li, and Y. Li, "Analysis for an improved nanomechanical microcantilever sensor on optical waveguides," *IEEE Access*, vol. 8, pp. 63856–63861, 2020.
[28] H. Gehring, A. Eich, C. Schuck, and W. H. P. Pernice, "Broadband out-of-plane coupling at visible wavelengths," *Opt. Lett.*, vol. 44, no. 20, pp. 5089–5092, 2019.
[29] H. Gehring, M. Blaicher, A. Eich, W. Hartmann, P. Varytis, K. Busch, C. Schuck, M. Wegener, and W. H. P. Pernice, "Broadband fiber-to-chip coupling in different wavelength regimes realized by 3D-structures," in *Proc. Conf. Lasers Electro-Opt.*, 2020, pp. 3–4.
[30] S. J. Choo, J. Kim, K. W. Lee, D. H. Lee, H.-J. Shin, and J. H. Park, "An integrated Mach–Zehnder interferometric biosensor with a silicon oxynitride waveguide by plasma-enhanced chemical vapor deposition," *Current Appl. Phys.*, vol. 14, no. 7, pp. 954–959, Jul. 2014.
[31] S. J. Choo, B.-C. Lee, S.-M. Lee, J. H. Park, and H.-J. Shin, "Optimization of silicon oxynitrides by plasma-enhanced chemical vapor deposition for an interferometric biosensor," *J. Micromech. Microeng.*, vol. 19, no. 9, Sep. 2009, Art. no. 095007.
[32] D. H. Lee, S. J. Choo, U. Jung, K. W. Lee, K. W. Kim, and J. H. Park, "Low-loss silicon waveguides with sidewall roughness reduction using a SiO_2 hard mask and fluorine-based dry etching," *J. Micromech. Microeng.*, vol. 25, no. 1, Jan. 2015, Art. no. 015003.

HYUN JIN JUNG was born in Asan, South Korea, in 1995. He received the B.S. degree in electrical engineering from Inha University, Incheon, South Korea, in 2020. He is currently pursuing the Ph.D. degree in electrical and electronic engineering with Korea University, Seoul, South Korea. His research interests include silicon based nanophotonic devices and optical waveguides.

UI SEOK JUNG was born in Asan, South Korea, in 1984. He received the B.S. and Ph.D. degrees in electrical and electronic engineering from Korea University, Seoul, South Korea, in 2009 and 2021, respectively. He is currently an Engineer with the NAND Flash, SK Hynix. His research interest includes silicon optical modulator utilizing a schottky diode for optical interconnects based optical waveguides.

BYUNG CHUL LEE (Member, IEEE) received the B.S. degree (summa cum laude) in electrical engineering from Korea University, in 2003, the M.S. degree in electrical engineering from the Korea Advanced Institute of Science and Technology (KAIST), in 2005, and the Ph.D. degree in electrical engineering from Stanford University, in 2015. He was a Research Scientist and a Senior Research Scientist at the Center for BioMicrosystems, Korea Institute of Science and Technology (KIST), Seoul, South Korea, from 2005 to 2021. He also joined as an Associate Professor at the KHU-KIST Department of Converging Science and Technology, Kyung Hee University, Seoul, in 2022. He is currently working as a Principal Research Scientist with the Bionics Research Center, KIST. He is also an Associate Professor with the Division of Bio-Medical Science and Technology, University of Science and Technology (UST), Seoul. His research interests include MEMS/NEMS technology for diverse biomedical applications such as bioelectronics, biosensors, micro-nanofluidics, micro-nanofabrications, and novel micromachined ultrasonic transducers and systems.

SOO JIN KIM received the B.S. degree from the Department of Electrical Engineering, Korea University, the M.S. and Ph.D. degrees in electrical engineering from Stanford University and performed Postdoctoral Research in materials science at Stanford University. He is currently an Associate Professor with the Department of Electrical Engineering, Korea University, Seoul, South Korea. His research interests include silicon photonics and nanophotonics for optical device applications.